A Journal of the Gesellschaft Deutscher Chemiker

Angewandte International Edition GDCh Chemie

www.angewandte.org

Accepted Article

Title: Activatable Polymeric Nanoprobe for Near-Infrared Fluorescence and Photoacoustic Imaging of T Lymphocytes

Authors: Yan Zhang, Qingqing Miao, and Kanyi Pu

To be cited as: *Angew. Chem. Int. Ed.* 10.1002/anie.202015116

Link to VoR: https://doi.org/10.1002/anie.202015116

WILEY-VCH

10.1002/anie.202015116

WILEY-VCH

RESEARCH ARTICLE

Activatable Polymeric Nanoprobe for Near-Infrared Fluorescence and Photoacoustic Imaging of T Lymphocytes

Yan Zhang,[#,*,a] Shasha He,[#b] Wan Chen,[c] Yinghua Liu,[c] Xuefei Zhang,[a] Qingqing Miao,[*,c] and Kanyi Pu[*,b]

[a] Prof. Y. Zhang, X. Zhang
National Engineering Research Centre for Nanomedicine, College of Life Science and Technology, Huazhong University of Science and Technology, 1037 Luoyu Road, Wuhan, 430074, P. R. China
E-mail: yan_zhang@hust.edu.cn

[b] Dr S. He, Prof. K. Pu
School of Chemical and Biomedical Engineering, Nanyang Technological University, 70 Nanyang Drive, Singapore 637457,
E-mail: kypu@ntu.edu.sg

[c] Prof. Q. Miao, W. Chen, Y. Liu
State Key Laboratory of Radiation Medicine and Protection, School for Radiological and Interdisciplinary Sciences (RAD-X), Collaborative Innovation Center of Radiation Medicine of Jiangsu Higher Education Institutions, Soochow University
Suzhou, 215123, P. R. China
E-mail: qqmiao@suda.edu.cn

Supporting information for this article is given via a link at the end of the document.

Abstract: Development of real-time non-invasive imaging probes to assess infiltration and activation of cytotoxic T cells (CTLs) is critical to predict the efficacy of cancer immunotherapy, which however remains challenging. We herein report an activatable semiconducting polymer nanoprobe (SPNP) for near-infrared florescence (NIRF) and photoacoustic (PA) imaging of a biomarker (granzyme B) associated with activation of CTLs. SPNP comprises a semiconducting polymer (SP) conjugated with a granzyme B cleavable and dye-labeled peptide as the side chain, both of which emit NIRF and PA signals. After systemic administration, SPNP passively targets the tumor and in-situ reacts with granzyme B to release the dye-labeled peptide, leading to decreased NIRF and PA signals from the dye but unchanged signals from the polymer. Such ratiometric NIRF and PA signals of SPNP correlate well with the expression level of granzyme B and intratumoral population of CTLs. Thus, this study not only presents the first PA probes for *in vivo* imaging of immune activation but also provides a molecular design strategy that can be generalized for molecular imaging of other immune-related biomarkers.

Introduction

Cancer immunotherapy that harnesses the host immune system to eliminate malignant cancer cells represents a promising clinical approach to treat various cancers.[1] Increasing evidences have revealed that the success of anti-cancer immunity strongly correlates with the presence of tumor-infiltrating T lymphocytes due to the pivotal role of T lymphocytes in antitumor immunity.[2] Thus, evaluation of the presence and activation of T lymphocytes is critical for monitoring cancer immunotherapeutic efficacy and predicting the cancer treatment outcome, which involves the biopsies assessment and anatomical measurement in clinical settings. While the invasive biopsies are often evaluated by post-therapeutic time scales and may poorly correlate with the clinic pathology; the imaging modalities including computed tomography (CT), magnetic resonance imaging (MRI), or positron emission tomography (PET), offer non-invasively diagnostic abilities.[3] However, these imaging modalities generally lack molecular sensitivity or specificity, which necessitates the development of alternative approaches to enable early and accurate assessment of the immune responses associated with T lymphocytes.

Molecular optical imaging enables early visualization and detection of subtle molecular abnormalities with high sensitivity and specificity.[4] Although fluorescence probes have been extensively exploited for imaging of cancer biomarkers, only few examples were reported for *in vivo* imaging of T lymphocytes, which include dye-iron oxide nanoparticles, and hemi-cyanine macromolecular reporter.[5] Moreover, fluorescence probes often encounter the tissue of shallow tissue penetration depth due to high photon absorption and scattering.[6] In contrast, photoacoustic (PA) imaging that integrates near-infrared (NIR) excitation with thermal-ultrasonic detection provides deeper tissue penetration (up to 12 cm) relative to fluorescence imaging.[7] Activatable PA imaging probes with biomarker-triggered signals offer measurable and quantifiable real-time information on pathological status at the molecular level.[8] Among many PA agents including gold nanoparticles,[9] two-dimensional materials,[10] carbon-based nanomaterials,[11] porphysomes,[7a, 12] dye-doped nanoparticles,[13] semiconducting polymer nanoparticles (SPN) are structurally versatile for construction of activatable PA imaging probes.[14] Till now, activatable PA probes have been used for *in vivo* imaging of a variety of biomarkers and biologically metabolites, including aberrant pH,[15] reactive oxygen species (ROS),[14a, 16] metal ions,[17] enzyme biomarker.[18] However, to the best of our knowledge, there are currently no activatable PA probes capable of real-time *in vivo* monitoring of T lymphocytes.

Herein, we report a semiconducting polymer nanoprobe (SPNP) that changes its NIR florescence (NIRF) and PA signals to detect granzyme B for real-time *in vivo* imaging of immune activation in the course of cancer therapy. Granzyme B, a serine protease in the granule of T lymphocytes, is chosen as the biomarker because its concentration is elevated in cytotoxic T lymphocytes (CTLs) and can be considered as a signature of immune activation.[19] SPNP is self-assembled from an amphiphilic semiconducting polymer (SP) conjugated with a dye-labeled and granzyme B cleavable peptide as the side chain (Scheme 1a and 1b). Intrinsically, SPNP has two sets of NIRF

10.1002/anie.202015116

and PA signals from the SP and the dye (IR800). In the presence of granzyme B, the dye-labeled peptide is cleaved and released from the SP core, leading to decreased NIRF and PA signals from IR800. In such a way, SPNP shows ratiometric NIRF and PA signals towards granzyme B (Scheme 1c). By virtue of its amphiphilicity and small size, SPNP can passively target the tumor and react with granzyme B after intravenous injection, permitting ratiometric NIR fluorescence and PA monitoring of T cell activation in the tumor of living mice.

Results and Discussion

To prepare the SPNP, mouse granzyme B-cleavable peptide, N-Acetyl-Pra-Ile-Glu(OtBu)-Phe-Asp(OtBu)-Ser(tBu)-Gly-OH (Pra-IE(OtBu)FD(OtBu) S(tBu)G-OH) was first synthesized by solid phase peptide synthesis, followed by reaction with ethylenediamine-N-Boc (EDA-N-Boc) to form Pra-IE(OtBu)FD(OtBu)S(tBu)G-EDA-N-Boc. Deprotection of OtBu, tBu and Boc groups of Pra-IE(OtBu)FD(OtBu)S(tBu)G-EDA-N-Boc afforded Pra-IEFDSG-EDA-NH_2. Then, the amino group of Pra-IEFDSG-EDA-NH_2 was reacted with IR800 to form Pra-IEFDSG-EDA-IR800. P1 was synthesized by palladium-catalyzed Suzuki polymerization of 2,6-dibromo-4,4-bis(6-bromohexyl)-4H-cyclopenta[2,1-b:3,4-b'] dithiophene (monomer1) and 1,3-benzothiadiazole-4,7-bis boronic acid pinacol ester (monomer 2). Then, the bromide groups of P1 were reacted with sodium azide to form P2. The azide groups of P2 underwent the copper(I)-catalyzed alkyne-azide cycloaddition (CAAC) reaction with Pra-IEFDSG-EDA-IR800 and PEG-alkyne sequentially to form the desired polymer (SPP). The chemical structures of peptide Pra-IEFD-SG, IR800 modified peptide, intermediate polymers and SPP were verified by proton NMR (^{1}HNMR) analysis (Figures S1-S4). Taking the ^{1}H NMR of SPP as an example, the peaks of the repeating unit of PEG (3.65 ppm), Pra-IEFDSG-EDA-IR800 (7.0–8.2 ppm, 1.0–3.0 ppm) and backbone segments (7.5–8.4 ppm) were detected.

The amphiphilicity of SPP enabled its spontaneous assembly into nanoparticles in aqueous solution, which was named as SPNP. The SPN without IR800-taged peptide (Pra-IEFD-SG-IR800) was synthesized as the control (SPNC). The average dynamic sizes of SPNC and SPNP were measured to be 20 and 25 nm, respectively (Figure 1a). The increased size was attributed to the conjugation of the IR800-taged peptide on the surface of SPNC, which was also confirmed by the decreased zeta potential from -1.28 mV for SPNC to -10.5 mV for SPNP (Figure S5). In addition, SPNP maintained its initial size distribution and absorption spectrum in phosphate buffered saline (PBS) after storage at 25°C for two months (Figure S5).

Prior to examine SPNP response towards granzyme B, the optical properties of its signal moieties, SPNC and IR800, were measured and compared (Figures 1b and 1c). As SPNC and IR800 had their respective absorption maxima at 660 nm and 785 nm, selective excitation was conducted to differentiate their fluorescence responses. SPNC had broad NIR fluorescence between 700 to 850 nm with a maximum at 820 nm upon excitation at 640 nm, and it was barely fluorescent upon excitation at 760 nm. In contrast, IR800 only showed strong NIR fluorescence peaked at 790 nm upon excitation at 760 nm. These results indicated the SP window (emission from 700 nm to 760 nm upon excitation at 640 nm) and the IR800 window (emission from 770~850 nm upon excitation at 760 nm) had negligible signal interference, and thus could be used for monitoring of the fluorescence responses of SPNP towards granzyme B.

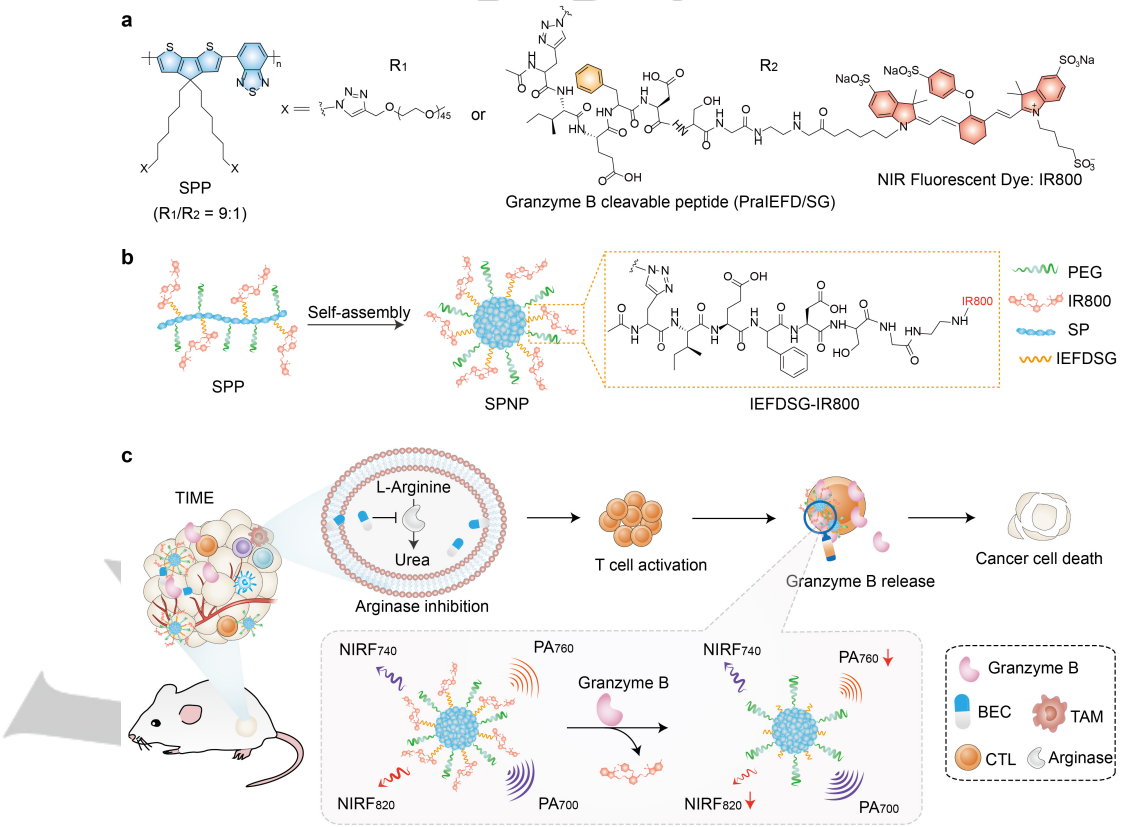

10.1002/anie.202015116

Scheme 1. Schematic illustration of SPNP for real-time imaging of CTL activation during cancer immunotherapy. (a) Chemical structure of SPP; (b) Schematic illustration of the formation of SPNP; (c) Mechanism of SPNP-based real-time NIRF and PA imaging of activated T lymphocytes *in vivo*.

The NIR fluorescence and PA responses of SPNP in the absence or presence of granzyme B were tested. SPNP had two absorption peaks maximum at 700 nm and 780 nm, corresponding to the SP backbone and IR800, respectively. After incubation of SPNP solution with granzyme B followed by ultracentrifugation for removal of low molecular weight substances, the absorption peak at 780 nm decreased while the intensity at 700 nm remained nearly the same, indicating the cleavage of Pra-IEFD-SG-IR800 by granzyme B (Figure 1d). This was further witnessed by fluorescence changes: the intensity at 740 nm for the SP window remained nearly the same; while the intensity at 820 nm for the IR800 window significantly decreased by 8-fold (Figure 1e). The ratiometric NIR fluorescence signal was defined as $NIRF_{740}/NIRF_{820}$, showing 4-fold enhancement after incubation with granzyme B (Figure 1g). Similarly, the PA signal of SPNP decreased only at 760 nm (corresponding to IR800) while remained nearly unchanged at 700 nm (corresponding to the SP) after incubation with granzyme B (Figure 1f), resulting in the ratiometric PA signal (PA_{700}/PA_{760}) enhancement by 1.4-fold relative to its inactive state (Figure 1g).

SPNP barely changed its NIR fluorescence in the presence of other enzymes including caspase-1, caspase-3, matrix metalloproteinase-2 (MMP-2), dipeptidyl peptidase (DPPI) and γ-glutamyl transferase (CGT), confirming its high selectivity towards granzyme B (Figure 1h). The enzymatic Michaelis-Menten constants (K_m) and catalytic rate constant (K_{cat}) of granzyme B towards SPNP were determined to be 31.7 μM and 0.007 s^{-1}, respectively (Figure 1i). Due to the steric hindrance from the nanoparticle, the catalytic efficiency (K_{cat}/K_m) was 221 $M^{-1}s^{-1}$, which was 14-fold lower than that of peptide conjugated dye.[5b] Together, SPNPs showed excellent activatable duplex NIR fluorescence/PA imaging properties towards granzyme B *in vitro*.

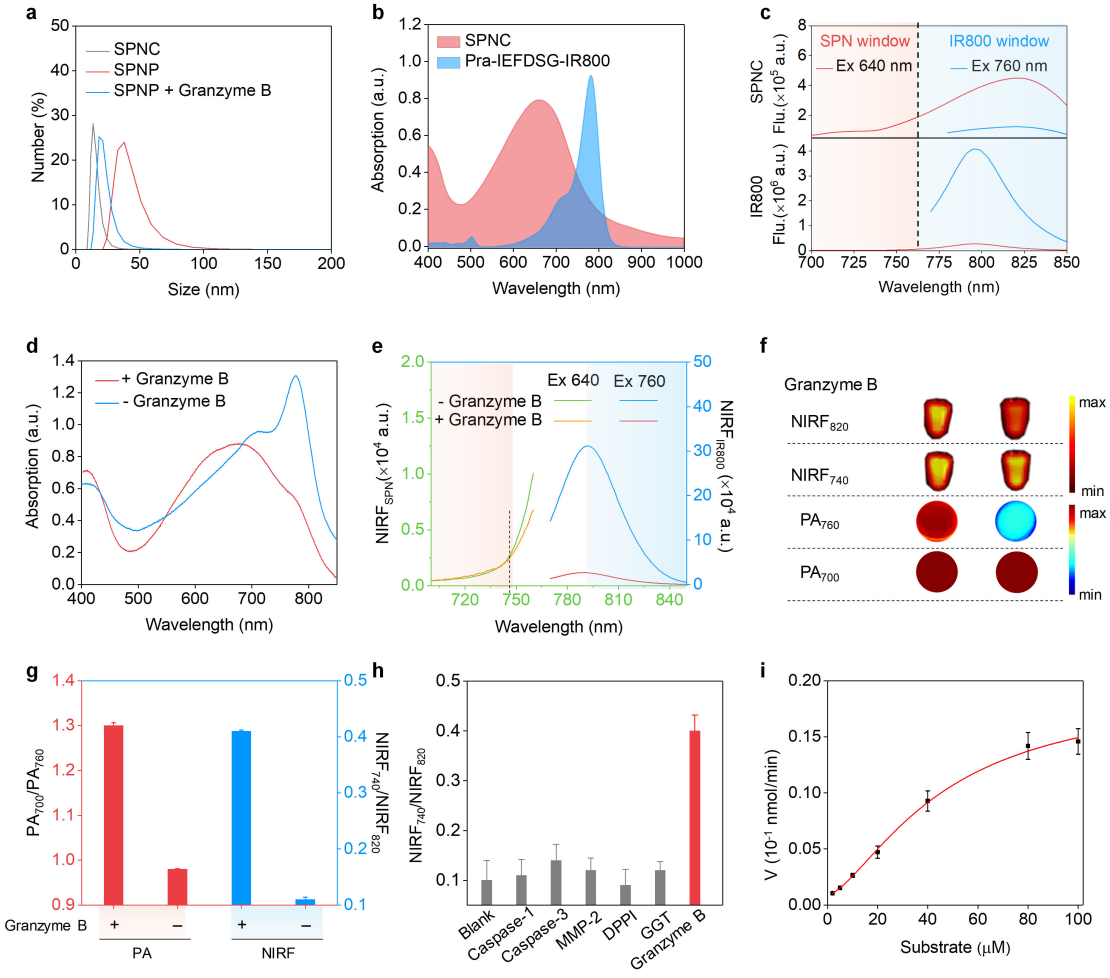

Figure 1. *In vitro* characterization of SPNP. (a) Dynamic light scattering (DLS) profiles of SPNC, SPNP and SPNP with granzyme B for 6 h. (b) UV/Vis absorption spectra of SPNC and Pra-IEFDSG-IR800. (c) Fluorescence spectra of SPNC and IR800 with excitations at 640 nm and 740 nm, respectively. (d) UV/vis absorption and (e) fluorescence spectra of SPNP in the absence or presence of mouse granzyme B (0.5 μg/mL) in tris(hydroxymethyl)aminomethane (Tris) (100 mM, pH 7.5) at 37 °C. SPNP solution (10 μg/mL SPN) was dissolved in Tris buffer, and granzyme B was added. After 2 h, the cleavage solution was collected, transferred to a centrifuge tube with a filter membrane (MwCO = 100 KDa), and placed in a centrifuge set at 10,000 rpm for 10 min. The residue on the filter membrane was resolved by Tris buffer for absorbance and fluorescence detection. (f) Fluorescence images of SPNP solution acquired at the emission of 740 nm upon excitation at 640 nm and the emission of 820 nm upon excitation at 740 nm; PA images of SPNP solution at 760 and 740 nm in the presence or absence of granzyme B. (g) The ratio of

NIRF at 740 nm to NIRF at 820 nm, and PA at 700 nm to PA at 760 nm of SPNP in the presence or absence of granzyme B. (h) The ratio of NIRF collected at 820 nm upon excitation at 740 nm to that at 740 nm upon excitation at 640 nm of SPNP solution was monitored in the presence of different enzymes. (i) Nonlinear regression analysis of cleavage rate V (nmol/min) of SPNP as a function of substrate concentration. Various concentrations of SPNP ([IR800]: 2, 5, 10, 20, 40, 80, or 100 μM) were incubated with mouse granzyme B (0.2 μg/mL) at 37 °C for 60 min in Tris buffer (100 mM, pH 7.5). After incubation, the mixture was measured by HPLC.

The ability of SPNP to detect granzyme B in cells was investigated in granzyme B-positive cytotoxic T cells ($CD8^+$ T cells) and granzyme B-negative 4T1 cancer cells. SPNC was utilized as the control. Note that both SPNP and SPNC showed negligible cell cytotoxicity towards $CD8^+$ T cells and 4T1 cells even at a high concentration of 200 μg mL^{-1} (Figure S6). After both nanoparticles were incubated with cells for 4 h, the cells and the supernatant were collected for confocal imaging at the SP window and fluorescence measurement at the IR800 window, respectively (Figure 2a). As shown in Figure 2b, intense NIR signals from the SP were observed in $CD8^+$ T cells and 4T1 cells after treatment of SPNC or SPNP. As the sizes of both nanoparticles were smaller than 50 nm, the possible cellular uptake mechanism could be pinocytosis. [20] Similar to SPNC, SPNP treated $CD8^+$ T cells showed a 1.6-fold higher NIRF intensity from the SP than that in 4T1 cells (Figure 2c). In contrast, the supernatant of SPNP-treated $CD8^+$ T cells had the NIRF signal of IR800 that was 23.5-fold higher than that of 4T1 cells (Figure 2d). Thus, these results confirmed that the Pra-IEFD-SG-IR800 fragment of SPNP was efficiently cleaved by granzyme B of $CD8^+$ T cells, allowing for sensitive detection of T cell activity.

The feasibility of SPNP for *in vivo* imaging of granzyme B after immunotherapeutic treatment was evaluated in 4T1 tumor bearing BALB/c mice model (Figure 3a). S-(2-boronoethyl)-l-cysteine hydrochloride (BEC) was used as an immunotherapeutic agent, known to elicit the activation of CTLs and helper T cells by inhibition of the activity of arginase in tumor microenvironment, was intravenously injected into the mice to activate T cells.[21] After intravenous SPNP injection, the fluorescence ($NIRF_{740}$) and PA signals (PA_{700}) from the SP in the tumor tissues increased gradually and the signals reached the similar maximum at 12 h post-injection time for both untreated and BEC-treated mice (Figures 3b and 3e). *Ex vivo* fluorescence imaging after NIRF and PA imaging further confirmed the similar biodistribution behavior of SPNP in untreated and BEC-treated mice, and they were mostly accumulated in the liver, spleen and tumor (Figure S7). In contrast, the signals ($NIRF_{820}$ and PA_{760}) from IR800 in tumors for untreated mice increased more rapidly than BEC-treated mice after SPNP injection and the $NIRF_{820}$ signals reached the maximum at 0.5 h post-injection time. Moreover, $NIRF_{820}$ signal was higher for untreated mice than that for BEC-treated mice at each time point till 36 h post-injection (Figure 3c). This indicated that SPNP was activated more in BEC-treated mice, leading to a more cleavage of IR800 in tumor. Quantitative analysis revealed that the $NIRF_{740}/NIRF_{820}$ and PA_{700}/PA_{760} for BEC-treated mice were increased continuously compared to those for untreated mice at each time point (Figures 3d and 3f). At 36 h post-injection, $NIRF_{740}/NIRF_{820}$ and PA_{700}/PA_{760} for BEC-treated mice was 2.25- and 1.2-fold higher than those for untreated mice, respectively. Noted that the $NIRF_{740}/NIRF_{820}$ for BEC-treated and untreated mice were slightly higher than those in *in vitro* measurements, which might be caused by the relative higher background interference at 740 nm relative to that at 820 nm *in vivo*. Considering nearly the same accumulation of SPNP in untreated and BEC-treated mice during the imaging process, the increased $NIRF_{740}/NIRF_{820}$ and PA_{700}/PA_{760} signals of SPNP were mainly attributed to the increased granzyme B levels in the tumors of BEC-treated living mice.

To validate whether the activated signals of SPNP correlated with the immunoactivation after the BEC-treatment, the level of granzyme B and population of T cell in tumors were measured

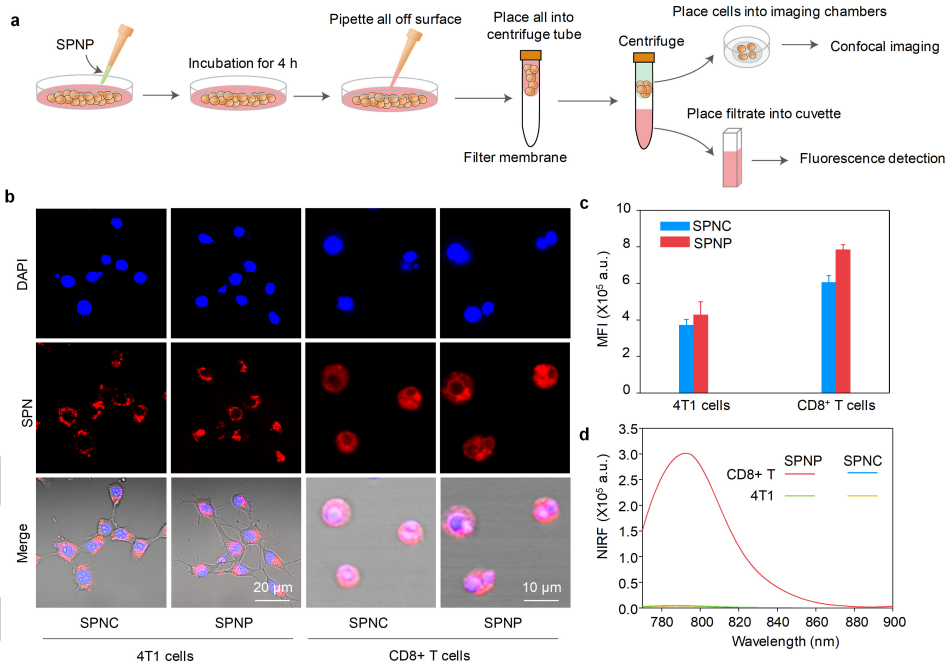

Figure 2. Detection of granzyme B in cell culture. (a) Schematic illustration of the experimental procedures for confocal fluorescence imaging and fluorescence detection of cell culture media. (b) Confocal fluorescence imaging and (c) mean fluorescence intensity (MFI) of 4T1 cells and $CD8^+$ T cells after 24 h incubation with

SPNP or SPNC ([SP] = 50 μg/mL). Emission at 740 nm; excitation at 640 nm. Blue fluorescence shows the cell nucleus stained with Hoechst and red fluorescence indicated the signals from the SP. (d) Fluorescence spectra of cell culture supernatant of 4T1 cells and $CD8^+$ T cells after 24 h incubation with SPNP ([SP] = 50 μg/mL) upon excitation at 760 nm.

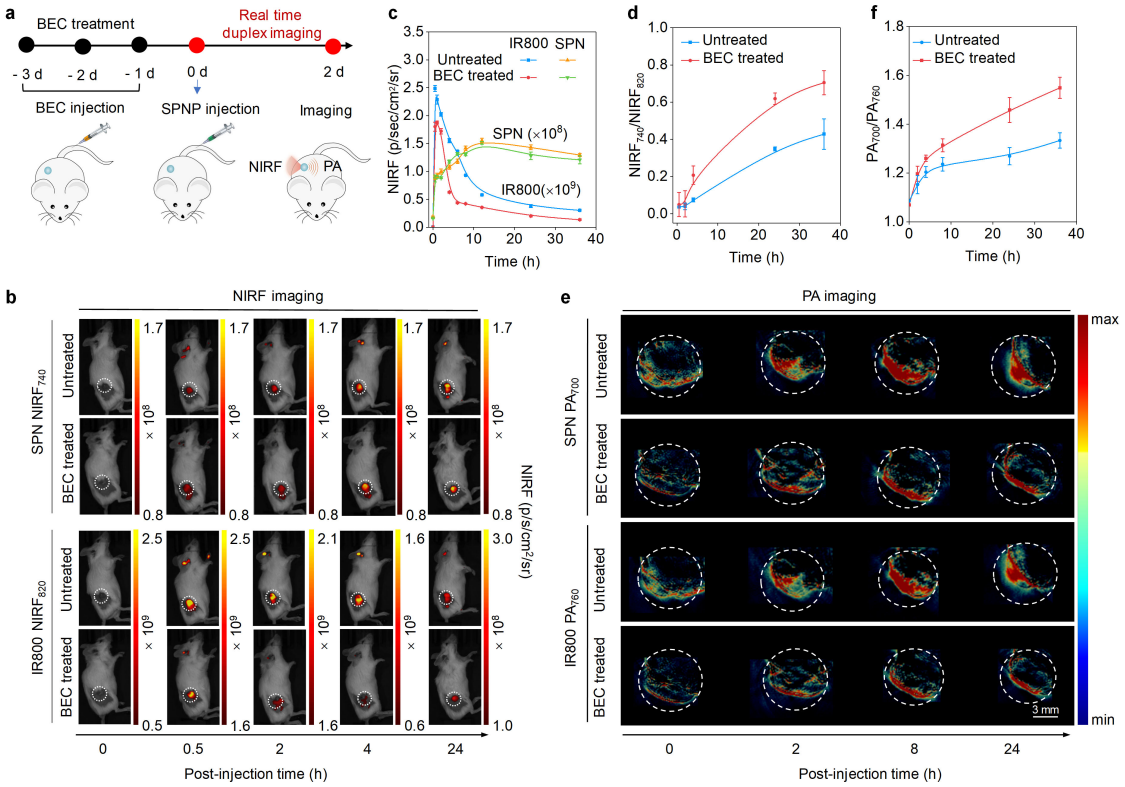

Figure 3. *In vivo* real-time NIR fluorescence and PA imaging of immune activation in living mice. (a) Schematic illustration of the timeline of BEC immunotherapy and real-time NIRF and PA imaging. (b) Representative NIRF images of untreated and BEC-treated 4T1-tumor-bearing BALB/c mice after intravenous injection of SPNP ([SP]=4 mg/kg) at different time points. (c) Quantification of fluorescence intensities of tumors as a function of post-injection time of SPNP in untreated or BEC-treated mice (n = 3). (d) The ratio of NIRF signal collected at 740 nm with excitation at 640 nm to that collected at 820 nm with excitation at 745 nm of tumors as a function of post-injection time of SPNP in untreated or BEC-treated mice. (e) Representative PA images of untreated and BEC-treated 4T1-tumor-bearing BALB/c mice after intravenous injection of SPNP at different timepoints. (f) The ratio of PA intensity at 700 nm to that at 760 nm of tumors as a function of post-injection time of SPNP in untreated or BEC-treated living mice.

by immunofluorescence staining and flow cytometry. The NIR fluorescence signal of SPNP in the tumor tissue was observed to located within the signal regions of granzyme B and $CD8^+$ T cells (Figures 4a and 4c); furthermore, the signals of granzyme B and $CD8^+$ T cells were 30- and 9-fold higher than those in the untreated mice, respectively (Figures 4b and 4d). Flow cytometry was then applied to quantitatively analyze the $CD4^+$ T cells, $CD8^+$ T cells and granzyme B-secreting cells in BEC-treated mice. $CD4^+$ T cells secret cytokines to enhance the ablation capability of $CD8^+$ T cells, and therefore, both cells can be utilized as the immunoactivation biomarkers. Compared to the untreated mice, $CD4^+$, $CD8^+$, and expression level of granzyme B were increased by 1.4-, 1.4-, 1.5-fold, respectively (Figures 4e and 4f). These results not only confirmed that BEC promoted the proliferation and activation of $CD8^+$ T cells, which increased the level of granzyme B to induce the signal changes of SPNP, but also validated that both *in vivo* NIR fluorescence and PA signals of SPNP correlated well with the immune activation in the tumor of mice.

Conclusion

In summary, we developed an activatable duplex probe (SPNP) for real-time imaging of the biomarker related to the activation of CTLs. SPNP comprised a SP backbone and granzyme B-responsive and dye-labeled peptide, both of which can function as the NIR fluorescence and PA imaging moieties. Only in the presence of granzyme B, could the efficient cleavage of the dye-labeled peptide of SPNP occur, resulting in diminished NIR fluorescence and PA signals of IR800 but unchanged signals from the SP. The sensitivity and specificity in conjunction with its passive tumor targeting ability allowed SPNP to effectively detect granzyme B in the tumors of living mice during cancer therapy. *Ex vivo* immunofluorescence staining and flow cytometry analyses further confirmed the correlation of NIR fluorescence and PA signals of SPNP with the expression level of granzyme B. Thus, SPNP represents the first activatable probe with NIR fluorescence/PA duplex signals for *in vivo* imaging of immune activation. Furthermore, the design of SPNP can be generalized for detection of other immune-related biomarkers simply by replacing the peptide linkage.

Acknowledgements

K.P. thanks Nanyang Technological University (Start-Up grant: M4081627) and Singapore Ministry of Education Academic Research Fund Tier 1 (2017-T1-002-134 RG147/17, 2019-T1-

002-045 RG125/19 and 2018-T1-001-173) and Academic Research Fund Tier 2 (MOE2018-T2-2-042) for the financial support. This work was also supported by the National Natural Science Foundation of China (81703031, 81672937 and 81627901).

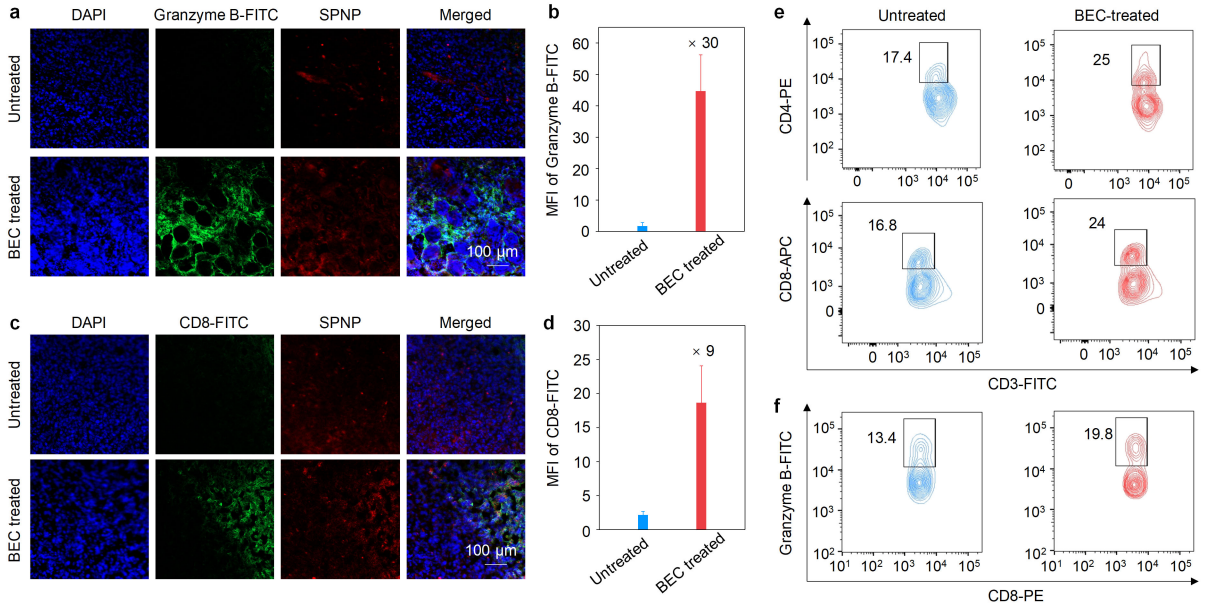

Figure 4. *Ex vivo* characterization of immune responses in isolated tumors. (a) Confocal fluorescence microscopy images and (b) quantification of granzyme B staining of tumor tissues from untreated and BEC-treated 4T1 tumor bearing mice at the end of imaging. Blue indicates the cell nucleus stained with 4',6-diamidino-2-phenylindole (DAPI), green indicates the signal of granzyme B staining. (c) Confocal fluorescence microscopy images and (d) quantification of CD8 staining of tumor tissues from untreated and BEC-treated 4T1 tumor bearing mice at the end of imaging. Blue indicates the cell nucleus stained with DAPI; green indicates the signal of CD8 staining. (e) Fluorescence-activated cell sorting (FACS) assay of tumor infiltrating T lymphocytes ($CD8^+$ and $CD4^+$) of 4T1 tumors at the end of imaging. (f) FACS assay of granzyme B expression of 4T1 tumors at the end of imaging.

Keywords: polymer nanoparticles; activatable probes; near-infrared fluorescence; photoacoustic imaging; immunotherapy

[1] K. M. Mahoney, P. D. Rennert, G. J. Freeman, *Nat. Rev. Drug Discov.* **2015**, 14, 561-584.

[2] a) J. Galon, D. Bruni, *Nat. Rev. Drug Discov.* **2019**, *18*, 197-218; b) C. Zhang, K. Pu. Chem. Soc. Rev., **2020**, *49*, 4234-4253.

[3] a) E. T. Ahrens, J. W. Bulte, *Nat. Rev. Immunol.* **2013**, 13, 755-763; b) J. A. Ronald, B. S. Kim, G. Gowrishankar, M. Namavari, I. S. Alam, A. D'Souza, H. Nishikii, H. Y. Chuang, O. Ilovich, C. F. Lin, R. Reeves, A. Shuhendler, A. Hoehne, C. T. Chan, J. Baker, S. S. Yaghoubi, H. F. VanBrocklin, R. Hawkins, B. L. Franc, S. Jivan, J. B. Slater, E. F. Verdin, K. T. Gao, J. Benjamin, R. Negrin, S. S. Gambhir, *Cancer Res.* **2017**, 77, 2893-2902; c) N. Pandit-Taskar, M. A. Postow, M. D. Hellmann, J. J. Harding, C. A. Barker, J. A. O'Donoghue, M. Ziolkowska, S. Ruan, S. K. Lyashchenko, F. Tsai, M. Farwell, T. C. Mitchell, R. Korn, W. Le, J. S. Lewis, W. A. Weber, D. Behera, I. Wilson, M. Gordon, A. M. Wu, J. D. Wolchok, *J. Nucl. Med.* **2020**, 61, 512-519.

[4] a) J. Huang, J. Li, Y. Lyu, Q. Miao, K. Pu, *Nat. Mater.* **2019**, *18*, 1133-1143; b) G. Hong, A. L. Antaris, H. Dai, *Nat. Biomed. Eng.* **2017**, *1*, 0010; c) Z. Shi, X. Han, W. Hu, H. Bai, B. Peng, L. Ji, Q. Fan, L. Li, W. Huang, *Chem. Soc. Rev.* **2020**, *49*, 7533-7567; d) Z. Hu, W. H. Chen, J. Tian, Z. Cheng, *Trends Mol. Med.* **2020**, *26*, 469-482.

[5] a) Q. D. Mac, D. V. Mathews, J. A. Kahla, C. M. Stoffers, O. M. Delmas, B. A. Holt, A. B. Adams, G. A. Kwong, *Nat. Biomed. Eng.* **2019**, *3*, 281-291; b) S. He, J. Li, Y. Lyu, J. Huang, K. Pu, *J. Am. Chem. Soc.* **2020**, *142*, 7075-7082.

[6] Q. Miao, C. Xie, X. Zhen, Y. Lyu, H. Duan, X. Liu, J. V. Jokerst, K. Pu, *Nat. Biotech.* **2017**, *35*, 1102-1110.

[7] a) U. Chitgupi, N. Nyayapathi, J. Kim, D. Wang, B. Sun, C. Li, K. Carter, W.-C. Huang, C. Kim, J. Xia, J. F. Lovell, *Adv. Mater.* **2019**, *31*, 1902279; b) Z. Yu, W. Hu, H. Zhao, X. Miao, Y. Guan, W. Cai, Z. Zeng, Q. Fan, T. T. Y. Tan, *Angew. Chem. Int. Ed.* **2019**, *58*, 8536-8540.

[8] a) J. Li, K. Pu, *Chem. Soc. Rev.* **2019**, *48*, 38-71; b) J. Li, K. Pu, *Acc. Chem. Res.* **2020,** *53*, 752-762.

[9] Z. Meng, X. Zhou, J. She, Y. Zhang, L. Feng, Z. Liu, *Nano Lett.* **2019**, *19*, 8109-8117.

[10] a) W. Tang, Z. Dong, R. Zhang, X. Yi, K. Yang, M. Jin, C. Yuan, Z. Xiao, Z. Liu, L. Cheng, *ACS Nano* **2019**, *13*, 284-294; b) L. Cheng, C. Yuan, S. Shen, X. Yi, H. Gong, K. Yang, Z. Liu, *ACS Nano* **2015**, *9*, 11090-11101; c) H. Lin, Y. Wang, S. Gao, Y. Chen, J. Shi, *Adv. Mater.* **2018**, *30*, 1703284.

[11] a) A. De La Zerda, C. Zavaleta, S. Keren, S. Vaithilingam, S. Bodapati, Z. Liu, J. Levi, B. R. Smith, T.-J. Ma, O. Oralkan, Z. Cheng, X. Chen, H. Dai, B. T. Khuri-Yakub, S. S. Gambhir, *Nat. Nanotech.* **2008**, *3*, 557-562; b) K. Yang, L. Hu, X. Ma, S. Ye, L. Cheng, X. Shi, C. Li, Y. Li, Z. Liu, *Adv. Mater.* **2012**, *24*, 1868-1872.

[12] a) J. F. Lovell, C. S. Jin, E. Huynh, H. Jin, C. Kim, J. L. Rubinstein, W. C. W. Chan, W. Cao, L. V. Wang, G. Zheng, *Nat. Mater.* **2011**, *10*, 324-332; b) M. H. Y. Cheng, K. M. Harmatys, D. M. Charron, J. Chen, G. Zheng, *Angew. Chem. Int. Ed.* **2019**, *58*, 13394-13399.

[13] a) Y. Zhang, M. Jeon, L. J. Rich, H. Hong, J. Geng, Y. Zhang, S. Shi, T. E. Barnhart, P. Alexandridis, J. D. Huizinga, M. Seshadri, W. Cai, C. Kim, J. F. Lovell, *Nat. Nanotech.* **2014**, *9*, 631-638; b) Y. Zhang, D. Wang, S. Goel, B. Sun, U. Chitgupi, J. Geng, H. Sun, T. E. Barnhart, W. Cai, J. Xia, J. F. Lovell, *Adv. Mater.* **2016**, *28*, 8524-8530; c) Y. Zhang, L. Feng, J. Wang, D. Tao, C. Liang, L. Cheng, E. Hao, Z. Liu, *Small* **2018**, *14*, 1802991.

[14] a) K. Pu, A. J. Shuhendler, J. V. Jokerst, J. Mei, S. S. Gambhir, Z. Bao, J. Rao, *Nat. Nanotech.* **2014**, *9*, 233-239; b) Y. Jiang, K. Pu, *Acc. Chem. Res.* **2018**, *51*, 1840-1849; c) Q. Miao, K. Pu, *Bioconjug. Chem.* **2016**, *27*, 2808-2823; d) J. Huang, K. Pu, *Angew. Chem. Int. Ed.* **2020**, *59*, 11717-11731; e) Y. Jiang, P. K. Upputuri, C. Xie, Y. Lyu, L. Zhang, Q. Xiong, M. Pramanik, K. Pu. *Nano letters*, **2017**, *17*, 4964-4969.

[15] a) Q. Miao, Y. Lyu, D. Ding, K. Pu, *Adv. Mater.* **2016**, *28*, 3662-3668; b) Q. Chen, X. Liu, J. Chen, J. Zeng, Z. Cheng, Z. Liu, *Adv. Mater.* **2015**, *27*, 6820-6827.

[16] a) J. Zhang, X. Zhen, P. K. Upputuri, M. Pramanik, P. Chen, K. Pu, *Adv. Mater.* **2017**, *29*, 1604764; b) C. J. Reinhardt, R. Xu, J. Chan, *Chem. Sci.* **2020**, *11*, 1587-1592.

10.1002/anie.202015116

[17] H. Li, P. Zhang, L. P. Smaga, R. A. Hoffman, J. Chan, *J. Am. Chem. Soc.* **2015**, *137*, 15628-15631.
[18] a) Y. Lyu, X. Zhen, Y. Miao, K. Pu, *ACS Nano* **2017**, *11*, 358-367; b) X. Zhen, J. Zhang, J. Huang, C. Xie, Q. Miao, K. Pu, *Angew. Chem. Int. Ed.* **2018**, *57*, 7804-7808; c) Q. Li, S. Li, S. He, W. Chen, P. Cheng, Y. Zhang, Q. Miao, K. Pu, *Angew. Chem. Int. Ed.* **2020**, *59*, 7018-7023.
[19] P. R. Hiebert, D. J. Granville, *Trends Mol. Med.* **2012**, *18*, 732-741.
[20] P. Foroozandeh, A. A. Aziz, *Nanoscale Res. Lett.* **2018**, *13*, 339.
[21] M. Pudlo, C. Demougeot, C. Girard-Thernier, *Med. Res. Rev.* **2017**, *37*, 475-513.

10.1002/anie.202015116

WILEY-VCH

RESEARCH ARTICLE

Table of Contents

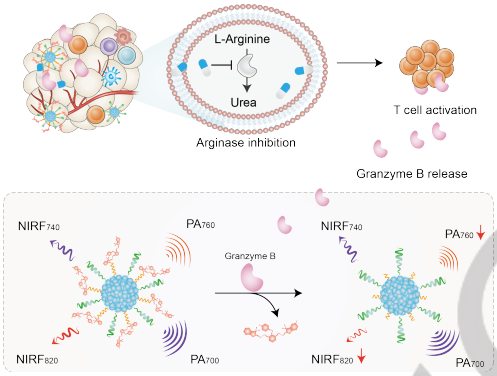

An activatable semiconducting polymer nanoprobe (SPNP) is synthesized for near-infrared fluorescence (NIRF) and photoacoustic (PA) detection of granzyme B, a biomarker related to activation of cytotoxic T lymphocytes. SPNP actively targets the tumor and reacts with granzyme B to release the dye-labeled peptide, leading to ratiometric NIRF/PA imaging of T lymphocytes during cancer immunotherapy.